

FASQ: Flexible Accelerated Subspace Quantization for Calibration-Free LLM Compression

Ye Qiao
yeq6@uci.edu
University of California, Irvine
Irvine, California, USA

Yian Wang
yianw11@uci.edu
University of California, Irvine
Irvine, California, USA

Zhiheng Chen
zhihenc5@uci.edu
University of California, Irvine
Irvine, California, USA

Hyoukjun Kwon
hyoukjun.kwon.p@gmail.com
University of California, Irvine
Irvine, California, USA

Sitao Huang
sitaoh@uci.edu
University of California, Irvine
Irvine, California, USA

Abstract

Compressing large language models (LLMs) for deployment on commodity GPUs remains challenging: conventional scalar quantization is limited to fixed bit-widths (e.g., 8/4/3-bit), offers only a few discrete compression points, and typically requires calibration data. We present FASQ (Flexible Accelerated Subspace Quantization), a calibration-free framework that applies product quantization to LLM weight matrices. By tuning two parameters, sub-vector size and codebook cardinality, FASQ exposes a continuous design space spanning 27–49% of the original FP16 model size, filling compression gaps that fixed-bit schemes cannot reach. On Meta-Llama-3-8B, FASQ surpasses 4-bit GPTQ and AWQ in accuracy (67.1–67.7 avg.) at 37–42% model size, with consistent results on Qwen3-8B and Qwen3.5-9B-Base. To make product quantization practical at inference time, we design custom CUDA kernels: a LUT-free direct-compute GEMV for decode and an output-stationary double-buffered LUT GEMM for prefill, both with split-K parallelism. On an RTX 3090, FASQ achieves 45.2 tok/s decode at effective 4-bit (2.56× memory reduction) and 51.8 tok/s at effective 3-bit (2.80×), both surpassing FP16 tensor-core performance (43.9 tok/s) and delivering 1.6–1.8× the throughput of AWQ, 2.2–2.5× of GPTQ, and 4.3–5.0× of RTN. FASQ is the only compressed method that accelerates decode beyond FP16, offering calibration-free compression, continuous size–quality trade-offs, and real-time inference on a single consumer GPU.

1 Introduction

Large language models (LLMs) have achieved remarkable performance across a wide range of tasks, yet their deployment is constrained by massive memory footprints and high inference costs. A single 7–9B parameter model requires 14–18 GB of GPU memory in FP16, often exceeding the capacity of commodity GPUs and limiting real-time serving scenarios. Post-training quantization (PTQ) has become the predominant solution: compared to other compression methods that require heavy fine-tuning or retraining, PTQ compresses pretrained weights to lower-precision representations without retraining [1–4].

However, existing PTQ methods share three fundamental limitations. First, scalar quantization is inherently restricted to discrete bit-widths (typically 8, 4, or 3 bits), each yielding a single fixed

compression point. Practitioners seeking intermediate trade-offs (e.g., between the 57% model size of INT8 and the 36% of INT4) have no available operating point. Second, state-of-the-art methods such as GPTQ [1], AWQ [2], and SmoothQuant [3] require representative calibration data to compute Hessian-based corrections, activation-aware scaling factors, or channel migration statistics, respectively. Obtaining such data may be impractical for proprietary or domain-specific models, and calibration procedures introduce a non-trivial step in the deployment pipeline. Third, scalar quantization requires explicit dequantization at inference time, reconstructing FP16 weights before each matrix multiplication. At standard 4-bit precision, custom kernels (e.g., AWQ-W4, GPTQ-W4) amortize this cost effectively, but at non-standard bit-widths where no optimized kernel exists, dequantization overhead can degrade latency by an order of magnitude [1, 2].

Product quantization (PQ), a classical technique from information retrieval that partitions vectors into sub-vectors and encodes each with a shared codebook, addresses all three limitations. By varying the sub-vector size and codebook cardinality, PQ exposes a continuous design space of compression rates. Codebook construction requires only k-means clustering on the weight distribution, eliminating external calibration data. Most importantly, PQ inference operates directly on compressed representations via table lookup, avoiding dequantization entirely and making latency independent of the compression level.

In this paper, we present FASQ (Flexible Accelerated Subspace Quantization), a post-training compression framework that applies multi-codebook product quantization to the linear layers of LLMs. FASQ replaces each FP16 weight matrix with a compact codebook of cluster centroids and a table of uint8 indices, then performs inference directly on these compressed representations: decode uses direct centroid-dot-product accumulation in registers, while prefill uses table-lookup-and-accumulate with shared-memory codebook caching. Through a systematic design space exploration, we show that FASQ covers compression rates from 27% to 49% of FP16 model size with fine granularity, filling the gap between fixed-bit scalar methods.

On Meta-Llama-3-8B, FASQ matches 8-bit quality (68.2 average accuracy across five zero-shot tasks) at 49% model size and exceeds 4-bit AWQ/GPTQ (67.1–68.2 avg.) at 37–42% model size, all without calibration data. These results generalize consistently to Qwen3-8B and Qwen3.5-9B-Base. To make PQ inference practical, we develop

custom CUDA kernels: a direct-compute GEMV kernel for decode that eliminates shared-memory lookup tables entirely, and a split-K GEMM kernel for prefill that maximizes GPU occupancy. The resulting engine achieves 45.2 tok/s decode throughput on an RTX 3090, surpassing FP16 (43.9 tok/s) at 2.56× less GPU memory. Because FASQ operates directly on compressed representations rather than dequantizing to FP16, its decode latency actually *improves* at higher compression, unlike scalar methods where non-standard bit-widths require entirely different kernel implementations.

Our contributions are as follows:

- We introduce FASQ, a calibration-free post-training compression framework that applies product quantization to LLM weights, exposing a continuous design space of compression vs. quality trade-offs unreachable by fixed-bit scalar methods.
- We evaluate FASQ across three modern LLM families (Llama-3, Qwen3, Qwen3.5) and show that it achieves accuracy competitive with state-of-the-art INT4 and INT8 quantization without any calibration data.
- We design two specialised CUDA kernels (a LUT-free direct-compute GEMV for decode and an output-stationary double-buffered LUT GEMM for prefill), making FASQ the only compressed method whose decode throughput surpasses FP16 tensor-core performance while reducing memory by 2.56–2.80×.
- We show that FASQ’s decode latency *improves* at higher compression (45.2 tok/s at eff. 4-bit, 51.8 tok/s at eff. 3-bit), inverting the latency penalty of scalar methods and delivering 1.6–1.8× the throughput of AWQ, 2.2–2.5× of GPTQ, and 4.3–5.0× of RTN.

2 Background and Motivation

2.1 Scalar Quantization for LLMs

Scalar quantization reduces the precision of individual weights from floating-point to a lower bit-width integer representation. Given a weight tensor w , the uniform affine mapping to b -bit integers is:

$$Q(w) = \text{clamp}\left(\left\lfloor \frac{w}{s} \right\rfloor + z, 0, 2^b - 1\right) \quad (1)$$

where $s = (\max(w) - \min(w)) / (2^b - 1)$ is the scale factor and $z = \lfloor -\min(w)/s \rfloor$ is the zero-point. While simple and hardware-friendly, this mapping suffers large quantization errors when outlier values dominate the dynamic range, which is common in LLM attention and feed-forward layers.

To mitigate outlier-induced error, state-of-the-art post-training quantization (PTQ) methods introduce calibration-based preprocessing. GPTQ [1] performs layer-wise quantization guided by a Hessian approximation computed from a calibration set, greedily rounding weights to minimize reconstruction error. AWQ [2] identifies salient weight columns via activation statistics and rescales them to fit the INT4 range more tightly. SmoothQuant [3] migrates quantization difficulty from activations to weights through per-channel scaling, enabling joint W8A8 quantization. These methods achieve strong quality at INT4 and INT8 but share three structural limitations. First, each bit-width yields a single fixed compression point; no intermediate operating points exist between, e.g., the 57%

model size of INT8 and the 36% of INT4. Second, all three require representative calibration data (Hessian statistics, activation distributions, or channel scaling factors) which may be unavailable for proprietary or domain-specific models. Third, scalar quantization requires explicit dequantization at inference time: integer weights must be reconstructed to FP16 before each matrix multiplication, and this cost is amortized only when a dedicated kernel exists for that bit-width. Group quantization partially addresses the first limitation by applying per-group scale factors within a fixed bit-width, but the compression range remains narrow and calibration is still required.

2.2 Product Quantization

Vector quantization (VQ) [5] quantizes entire vectors rather than individual scalars. A codebook of K centroids is learned via k-means, and each input vector is replaced by the index of its nearest centroid. By capturing correlations within vectors that element-wise methods ignore, VQ yields lower reconstruction error at equivalent storage.

Product quantization (PQ) [6] scales VQ to high-dimensional spaces by partitioning each vector into N_{ss} sub-vectors and maintaining an independent codebook per partition. The composite codebook has $K^{N_{ss}}$ implicit entries while storing only $K \times N_{ss}$ centroids, making PQ exponentially more expressive than a single-codebook VQ of the same size. Codebook learning requires only k-means on the data itself, with no external labels or calibration inputs, and the resulting representation is a compact pair of tables: centroids (FP16) and indices (uint8).

Several works have applied PQ or lookup-based computation to neural network inference. Maddness [7] replaces multiply-accumulate operations with learned hash lookups, and PECAN [8] uses content-addressable memory for mapping, but both target activations rather than weight compression. DPQ [9], LUT-NN [10], and PQA [11] apply PQ to network weights or LLM inference but rely on naïve dequantization without custom GPU kernels, incurring substantial inference overhead. LUT-DLA [12] adds a design-space search for hardware co-optimization but targets FPGA rather than commodity GPUs.

Orthogonally, table-lookup engines on edge FPGAs [13–15] and efficient NAS for constrained platforms [16–20] target custom hardware or extreme quantization, while quantization-induced positional encoding degradation [21, 22] further motivates calibration-free approaches. None of these works provide flexible, GPU-efficient compression with a continuous quality and size tradeoff.

3 FASQ

This section describes the FASQ quantization procedure (Section 3.1.1), reconstruction-free inference (Section 3.1.2), and the resulting design space (Section 3.2).

3.1 FASQ Methodology

3.1.1 Quantization. FASQ partitions each weight matrix $W \in \mathbb{R}^{d \times d'}$ into N_{ss} subspaces along a chosen *subspace dimension* dim_{ss} . The partitioning can be applied along either the row (d) or column (d') axis; we denote this choice by a binary variable dim (0 for rows, 1 for columns). The complementary axis is the *datapoint dimension*

Algorithm 1 FASQ Quantization Process

Require: Weight matrix W with shape (d, d') , number of clusters K_s , number of subspaces N_{ss} , subspace dimension dim .

Ensure: Cluster table $T_{cluster}$, index table T_{index}

- 1: **let** dim_{dp} be the data point dimension.
- 2: $dim_{ss} \leftarrow d$ if $dim \leftarrow 0$ else d' , dim_{dp} be the number of data points
- 3: $SZ_{ss} \leftarrow \frac{dim_{ss}}{N_{ss}}$
- 4: Initialize $T_{cluster} \in \mathbb{R}^{N_{ss} \times K_s \times SZ_{ss}}$, $T_{index} \in \mathbb{R}^{N_{ss} \times ndp}$
- 5: **parallel for** $ss_i \leftarrow 1$ to N_{ss} **do**
- 6: $(C, I) \leftarrow \text{KMeans}(W_{ss_i}, K_s)$
- 7: $T_{cluster}[ss_i] \leftarrow C$
- 8: $T_{index}[ss_i] \leftarrow I$
- 9: **end parallel for**
- 10: **return** $T_{cluster}, T_{index}$

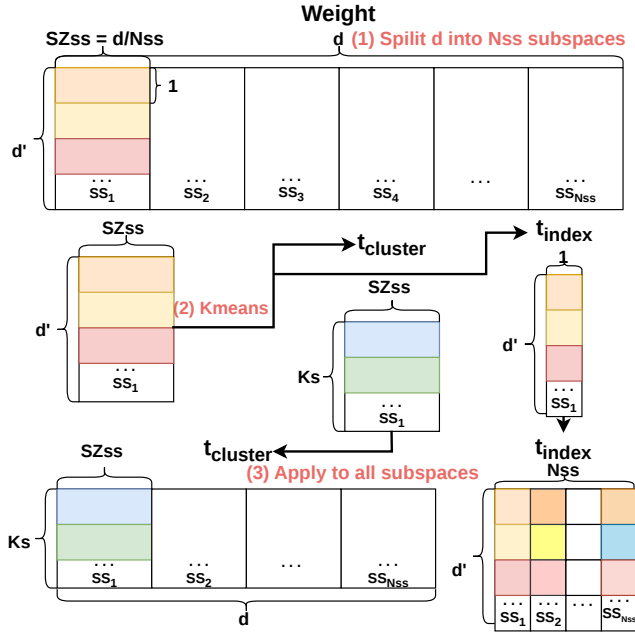


Figure 1: Example FASQ quantization process with $N_{ss} = 4$. ①: The weight matrix is split into N_{ss} subspaces along the chosen dimension; ②: K-means clustering is applied independently within each subspace; ③: Centroids and indices are stored as the compressed representation.

dim_{dp} . Each subspace slice has shape:

$$W_{ss} \in \begin{cases} \mathbb{R}^{\frac{d}{N_{ss}} \times d'}, & \text{if } dim = 0 \\ \mathbb{R}^{d \times \frac{d'}{N_{ss}}}, & \text{if } dim = 1 \end{cases} \quad (2)$$

with subspace size $SZ_{ss} = dim_{ss}/N_{ss}$.

Within each subspace, we run k-means with K_s clusters along dim_{dp} , producing a centroid table $T_{cluster}^{ss} \in \mathbb{R}^{K_s \times SZ_{ss}}$ and an index vector $T_{index}^{ss} \in \{0, \dots, K_s - 1\}^{dim_{dp}}$. Aggregating over all subspaces yields the full codebook $T_{cluster} \in \mathbb{R}^{N_{ss} \times K_s \times SZ_{ss}}$ and the index table $T_{index} \in \{0, \dots, K_s - 1\}^{N_{ss} \times dim_{dp}}$. Because k-means operates solely on the weight distribution, **no calibration data is required**. The

complete procedure is given in Algorithm 1 and illustrated in Figure 1.

3.1.2 Inference. A naïve approach reconstructs the full weight matrix via index lookups and then calls a standard matrix multiplication. However, reconstruction temporarily materializes the entire FP16 weight matrix, negating the memory savings of quantization.

We instead perform **reconstruction-free** inference that operates directly on the codebook and index tables without ever materializing the weight matrix. The core observation is that the output of a PQ-compressed linear layer can be decomposed as:

$$o_j = \sum_{ss=1}^{N_{ss}} \text{dot}(x_{ss}, T_{cluster}[ss, T_{index}[ss, j]]) \quad (3)$$

where x_{ss} is the input slice corresponding to subspace ss . Each term requires only a single centroid fetch (indexed by T_{index}) and a small dot product of dimension SZ_{ss} ; no full row of the weight matrix is ever formed.

We specialize the implementation into two kernels tailored to the two LLM inference phases:

- **Decode (GEMV):** During autoregressive token generation, the input is a single vector ($B=1$). Each thread owns one output element and directly computes Equation 3 by iterating over subspaces, fetching the relevant centroid on the fly, and accumulating the dot product in a register. No shared-memory lookup table is needed, because each thread uses only one of the K_s centroids per subspace.
- **Prefill (GEMM):** During prompt processing, many input tokens ($L \gg 1$) share the same weight. Here, precomputing a shared-memory lookup table $LUT_{ss}[k] = x_l \cdot T_{cluster}[ss, k]^T$ for all K_s centroids amortizes the cost across the L output rows, and each thread accumulates results for multiple output features via indexed gathers from the LUT.

Both approaches are inherently dequantization-free: the compressed codebook and index tables are consumed directly, with no intermediate FP16 weight materialization. The detailed kernel designs and CUDA-level optimisations are presented in section 4.

3.2 FASQ Design Space

FASQ targets the linear layers of transformer models, which account for the vast majority of parameters. We assume the baseline model stores weights in FP16 (16 bits per element).

FASQ compresses each layer by replacing the full $dim_{ss} \times dim_{dp}$ weight matrix with two compact structures: (1) a *codebook* of $N_{ss} \times K_s$ centroids, each of dimension SZ_{ss} , shared across all dim_{dp} datapoints; and (2) an *index table* that stores one $\lceil \log_2 K_s \rceil$ -bit integer per datapoint per subspace instead of SZ_{ss} FP16 values. The per-layer footprint is therefore:

$$S_{fasq}^{layer} = \underbrace{16 \times K_s \times dim_{ss}}_{\text{codebook (shared)}} + \underbrace{\lceil \log_2 K_s \rceil \times N_{ss} \times dim_{dp}}_{\text{index table}} \quad (4)$$

The codebook cost is independent of dim_{dp} and therefore negligible at typical model dimensions (e.g. $<1\%$ of layer size at $K_s=256$, $d=4096$). Compression is dominated by the index table, which replaces each FP16 weight group with a single $\lceil \log_2 K_s \rceil$ -bit index.

Algorithm 2 FASQ GEMV Kernel (Decode, $B=1$)

Require: $x \in \mathbb{R}^{F_{in}}$, $T_{cluster} \in \mathbb{R}^{N_{ss} \times K_s \times SZ_{ss}}$
Require: $T_{index} \in \{0, \dots, K_s - 1\}^{N_{ss} \times F_{out}}$
Ensure: $o \in \mathbb{R}^{F_{out}}$

- 1: $o \leftarrow \mathbf{0}$; auto-tune nss_splits for ~ 8 blks/SM
- 2: **parallel for** thread (j, z) : $j \in [0, F_{out}]$, $z \in [0, nss_splits]$ **do**
- 3: $acc \leftarrow \mathbf{0}$ ▷ register
- 4: **for** ss in split z 's subspace range **do**
- 5: $k \leftarrow T_{index}[ss, j]$ ▷ 1 B index
- 6: $c \leftarrow T_{cluster}[ss, k]$ ▷ centroid
- 7: $acc += \text{dot}(x_{ss}, c)$ ▷ SZ_{ss} FMAs
- 8: **end for**
- 9: $\text{atomicAdd}(o[j], acc)$ ▷ 1 atomic/thread
- 10: **end parallel for**

For a given model and choice of dim , the layer size is determined entirely by K_s and N_{ss} .

The model-level size ratio aggregates all FASQ-quantized linear layers together with uncompressed auxiliary components (embeddings, LayerNorm):

$$\text{Size\%} = \frac{S_{\text{fasq}}}{S_{\text{base}}} \times 100\% \quad (5)$$

We additionally apply deduplication by removing repeated centroids within each subspace; hence Equation 4 is an upper bound. In our tables, the effective bitwidth $\#W$ reports only the index rate $\lceil \log_2 K_s \rceil / SZ_{ss}$, excluding codebook overhead, analogous to how integer quantization methods report precision without counting group-wise scaling factors.

We define the FASQ design space as:

$$\text{Design Space} = \{K_s, N_{ss}, dim\} \quad (6)$$

operating on FP16 weights, the standard deployment format for pretrained LLMs. By sweeping SZ_{ss} from 1 (element-wise k-means) to dim_{ss} (full vector quantization) and K_s from 1 to dim_{dp} , FASQ traces a continuous Pareto front of compression rate versus model quality (Section 5.2).

4 FASQ Acceleration

LLM inference consists of two phases: *prefill*, which processes the prompt via a batched GEMM, and *decode*, which generates tokens one at a time via GEMV. The two phases impose different parallelism requirements, so we design a dedicated CUDA kernel for each. We present the designs of both kernels, an ablation study of the key optimisations, and a sensitivity analysis of FASQ parameters. All microbenchmark measurements are on a single 4096×4096 linear layer, RTX 3090.

A natural approach to PQ inference is to precompute a *lookup table* (LUT) of all K_s dot products per subspace in shared memory, then gather results by index (Equation 3). Whether this pays off depends on the batch size: at $B=1$ each thread uses only one of the K_s entries, wasting the table; at large L , many tokens amortize the build cost. This tradeoff drives our two-kernel design.

4.1 GEMV Kernel for Decode

Algorithm 3 FASQ GEMM Kernel (Prefill, $L > 1$)

Require: $X \in \mathbb{R}^{L \times F_{in}}$, $T_{cluster}$, T_{index}
Ensure: $O \in \mathbb{R}^{L \times F_{out}}$

- 1: $O \leftarrow \mathbf{0}$; auto-tune nss_splits for ~ 6 blks/SM
- 2: **parallel for** block (l, z) : $l \in [0, L]$, $z \in [0, nss_splits]$ **do**
- 3: Alloc double-buffered $lut_0, lut_1 \in \mathbb{R}^{K_s}$ in shmem
- 4: Each thread owns $acc[0:F_{pt}-1] \leftarrow \mathbf{0}$ ▷ $F_{pt}=16$
- 5: **Build** $lut_0[k] \leftarrow \text{dot}(X[l]_{ss0}, T_{cluster}[ss_0, k])$, $\forall k$
- 6: $___syncthreads()$
- 7: **for** each subspace ss in split z 's range **do**
- 8: $cur \leftarrow lut_{i \bmod 2}$; $nxt \leftarrow lut_{(i+1) \bmod 2}$
- 9: **Build** nxt for next subspace ▷ overlaps reads
- 10: **for** $p = 0$ to $F_{pt} - 1$ **do**
- 11: $acc[p] += cur[T_{index}[ss, j_p]]$ ▷ LUT gather
- 12: **end for**
- 13: $___syncthreads()$ ▷ 1 barrier/subspace
- 14: **end for**
- 15: Store: direct fp16 if $nss_splits=1$, else atomicAdd
- 16: **end parallel for**

During autoregressive decode, the input is a single token. A naïve LUT approach builds K_s partial dot products per subspace in shared memory, but each thread consumes only 1 of the K_s entries; at $K_s=256$, **99.6% of the LUT is wasted**.

Our GEMV kernel (Algorithm 2) eliminates the LUT entirely, as illustrated in Figure 2. Each thread owns a single output element o_j and iterates over its assigned subspaces. For each subspace ss , the thread reads the index $k = T_{index}[ss, j]$ (1 byte), fetches the corresponding centroid $T_{cluster}[ss, k]$ ($SZ_{ss} \times 2$ bytes), computes the dot product with the input slice using SZ_{ss} fused multiply-add (FMA) operations, and accumulates the result in a register (Figure 2, right). After all subspaces are processed, a single atomicAdd writes the partial sum to global memory.

Split-K parallelism. To maximise GPU occupancy, we partition the N_{ss} subspaces across the grid's z-dimension (Figure 2, left). The auto-tuner targets ~ 8 blocks per SM, yielding $K_{\text{split}} = \lceil (N_{SM} \times 8) / (B_s \times \lceil F_{out}/128 \rceil) \rceil$ splits (~ 21 on RTX 3090). Each thread performs a single atomicAdd at the end of its subspace chunk, compared with N_{ss} atomics per element in a subspace-stationary design.

Key properties. This design uses **zero shared memory** and **zero synchronisation barriers**, enabling up to 12 resident blocks per SM (versus 1 for the 32 KB LUT design). At $SZ_{ss}=2$, the centroid is a single half2 load; the entire subspace codebook ($K_s \times SZ_{ss} \times 2 = 1$ KB) fits in L1 and is reused across the warp. The dominant cost is reading the index table: $N_{ss} \times F_{out} \times 1 \text{ B} = 8$ MB vs. cuBLAS FP16's 32 MB weight read, yielding a 4× memory traffic reduction that explains why our kernel (32 μs) outperforms cuBLAS (45 μs).

4.2 GEMM Kernel for Prefill

During prefill, L input tokens share the same weight. Building a K_s -entry LUT per subspace now pays off: the L tokens each reuse the same table, amortizing the build cost by a factor of L . Our GEMM kernel assigns one sequence position to each block row (grid- x) and iterates serially over subspaces. For each subspace, a K_s -entry

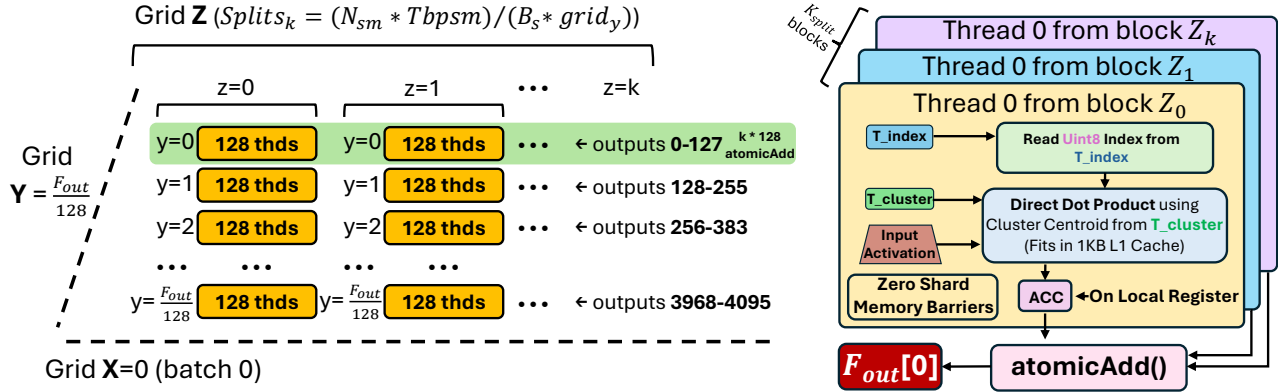


Figure 2: FASQ GEMV kernel design for autoregressive decode ($B=1$). Left: the 3D grid layout, where grid- $y = \lceil F_{out}/128 \rceil$ partitions outputs into 128-thread blocks and grid- z implements Split-K by dividing N_{ss} subspaces across K_{split} blocks (auto-tuned for ~ 8 blocks/SM). Right: per-thread computation, each thread reads a uint8 index from T_{index} , performs a direct dot product with the corresponding centroid from $T_{cluster}$ (fitting in 1 KB L1 cache), and accumulates in a local register with zero shared memory or barriers. Partial sums from all K_{split} blocks merge via a single `atomicAdd` per output element.

Table 1: Kernel design ablation on RTX 3090 (4096×4096 layer). Each row adds one optimisation cumulatively.

	Optimisation	GEMV ($B=1, \mu s$)	GEMM ($L=128, ms$)
(a)	cuBLAS FP16 (tensor core)	45	0.08
(b)	Subspace-stationary LUT (both)	142	5.11
(c)	+ Output-stationary; half2, fused f2h	94	2.75
(d)	+ LUT-free direct compute, split-K (GEMV)	32	–
(e)	+ Split-K, double-buffered LUT (GEMM)	–	2.02

LUT is built cooperatively by all threads (each thread computes $\lceil K_s/256 \rceil$ entries), then each thread looks up 16 output features from the LUT and accumulates results in registers.

Split-K along N_{ss} . At short sequences ($L=32-128$), we split the N_{ss} -loop across the grid z -dimension to increase block count. At $L=128$ the auto-tuner selects ~ 4 splits, boosting blocks from 128 to 512 (6.2/SM) and reducing latency by 1.35×; at large L , splits are disabled with zero overhead.

Double-buffered LUT. Two LUT slots reside in shared memory: while accumulators read from `lut_cur`, `lut_next` is built for the next subspace, requiring only one `__syncthreads()` per iteration. Each slot is padded to $K_s+1=257$ floats (2 KB for the pair) for bank-conflict avoidance.

4.3 Kernel Design Ablation

Table 1 ablates each optimisation cumulatively on a single 4096×4096 layer.

The baseline PQ kernel (b) uses a shared-memory LUT with subspace-stationary parallelism, where each block owns one subspace and iterates over all output elements. Switching GEMM to an output-stationary design (each thread owns output features, iterates over subspaces) and adding half2 vectorised loads, fused float-to-half conversion, and PyTorch’s caching allocator (c) yields a 1.5× GEMV and 1.9× GEMM speedup. Eliminating the LUT entirely

and adding split-K parallelism along N_{ss} (d) achieves a further 2.9× GEMV speedup, bringing decode latency **below** cuBLAS FP16; the GEMM kernel retains its LUT since the cost is amortized across L tokens. Finally, GEMM split-K (also along N_{ss} , but retaining the LUT) and double-buffered LUT (e) provide a 1.35× prefill speedup at short sequence lengths.

4.4 Sensitivity Analysis

Codebook size (K_s). As K_s varies from 16 to 256 (Figure 3a), GEMV latency rises only from 25.3 to 37.4 μs (1.48×) because the dominant cost, reading the index table ($N_{ss} \times F_{out}$ bytes), is independent of K_s . **All K_s values remain faster than cuBLAS FP16** (45.5 μs), so compression quality can be tuned freely.

Sub-vector size (SZ_{ss}). $SZ_{ss}=1$ doubles the index table to 16 MB and disables half2 vectorisation (134.7 μs , 3.0× cuBLAS). $SZ_{ss}=2$ halves index traffic and enables half2, reaching 36.7 μs (0.81× cuBLAS); larger values give diminishing returns. We use $SZ_{ss}=2$ throughout.

Sequence length scaling. Split-K provides the largest GEMM benefit at short sequences (4.5× at $L=32$), tapering to 1.01× at $L \geq 512$ where blocks already saturate the GPU. The FASQ GEMM is $\sim 26-28\times$ slower than cuBLAS FP16 at large L (tensor-core gap); however, prefill runs once per request while decode dominates interactive serving (Figure 3c).

Batch size. At $B=1$, our GEMV kernel is 1.2× **faster** than cuBLAS FP16, as the 4× memory traffic reduction outweighs the lack of tensor cores. As B grows, cuBLAS scales more favourably via tensor-core GEMM; an adaptive dispatch switching kernels at larger B is left for future work.

5 Experiments

We evaluate FASQ on an NVIDIA RTX 3090 GPU, measuring model quality, compressed model size, and end-to-end inference latency with our custom CUDA kernels.

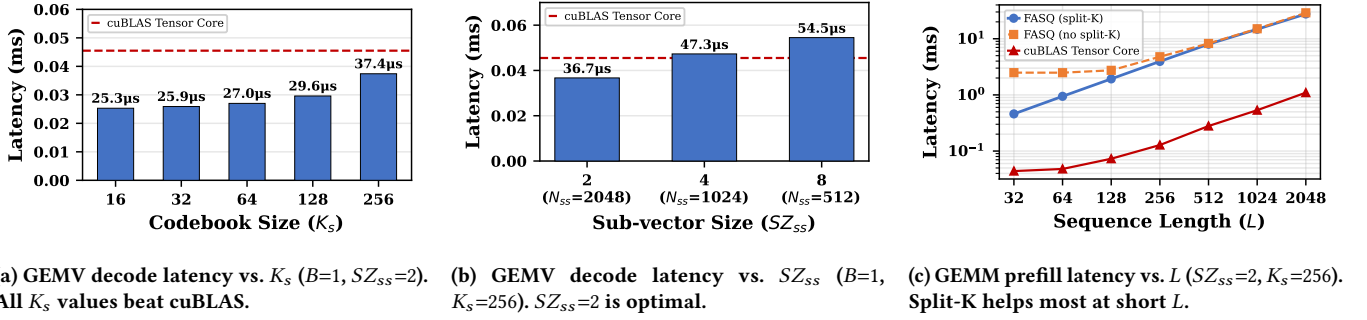


Figure 3: Sensitivity analysis of FASQ kernels on a single 4096×4096 layer (RTX 3090).

5.1 Experimental Settings

5.1.1 Baselines. We compare against five post-training quantization methods: GPTQ [1] (Hessian-guided INT4/INT3), AWQ [2] (activation-aware weight quantization), SmoothQuant [3] (joint weight-activation quantization at W8A8, W6A6, and W4A4), QuIP [23] (incoherence processing before quantization), and RTN (round-to-nearest, no calibration). All baselines except RTN require calibration data; FASQ does not.

5.1.2 LLM Workloads. We evaluate on three modern model families: Meta-Llama-3-8B [24], Qwen3-8B [25], and Qwen3.5-9B-Base [25]. For scalability analysis, we additionally evaluate on LLaMA-2 [26] 7B and 13B. We measure perplexity on the WikiText-2 test set [27] and zero-shot accuracy on five commonsense reasoning tasks: ARC-easy and ARC-challenge [28], HellaSwag [29], PIQA [30], and Winogrande [31].

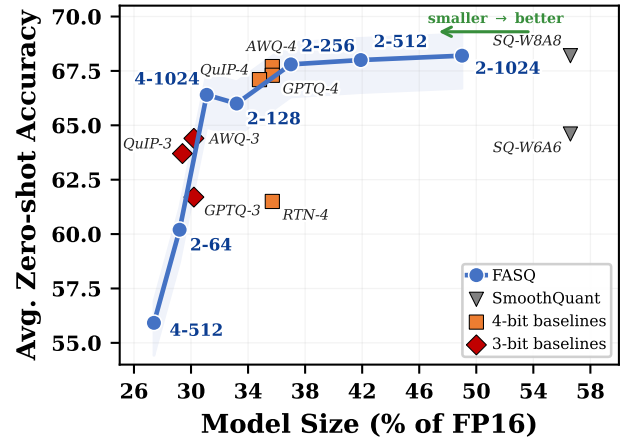
5.1.3 Configurations. FASQ is parameterized by sub-vector size SZ_{ss} and codebook size K_s , written as $SZ_{ss}\text{-}K_s$ (e.g., 2-256 denotes $SZ_{ss}=2, K_s=256$).

5.1.4 Methodology. We reproduced baselines using official implementations of GPTQ¹, AWQ², and SmoothQuant³. All evaluations use lm-evaluation-harness [32]. Compression rates are measured from stored model weight size only, excluding activations and KV caches. End-to-end latency is measured on Meta-Llama-3-8B with prompt length 128 and generation length 128. All latency measurements use CUDA event timers with warmup.

5.2 Design Space Exploration

As discussed in Section 3.2, Equation 4 defines the memory footprint of a single FASQ-quantized linear layer. We sweep $SZ_{ss} \in \{1, 2, 4, 8\}$ and $K_s \in \{64, 128, 256, 512, 1024, 2048\}$ on Meta-Llama-3-8B to map the full design space. All experiments use $dim=0$ (quantization along the output dimension), which we found consistently outperforms $dim=1$ across all configurations.

Figure 4 plots each configuration by model size (% of FP16) versus average zero-shot accuracy, with scalar quantization baselines overlaid for reference. Configurations with $SZ_{ss} \leq 2$ form a smooth

Figure 4: Pareto front of FASQ design space on Meta-Llama-3-8B. Each point is one (SZ_{ss}, K_s) configuration. FASQ with $SZ_{ss} \leq 2$ traces a smooth front that matches or exceeds scalar baselines across the full size range.

Pareto front spanning 27–49% of FP16 size, demonstrating the *continuous* compression–quality tradeoff that FASQ uniquely offers, in contrast to scalar methods that are locked to discrete bit-widths. The best FASQ configs on this front (2-512, 2-1024) match or exceed 4-bit baselines at comparable model sizes. Configurations with $SZ_{ss} \geq 4$ fall below the Pareto front, confirming that the expressive sweet spot lies at $SZ_{ss} \in \{1, 2\}$.

5.3 Model Quality Results

5.3.1 Cross-Model Generalization. Table 3 shows that FASQ generalizes across three diverse model families. Across Llama-3-8B, Qwen3-8B, and Qwen3.5-9B-Base, the same configurations produce consistently low perplexity degradation. For example, the 2-1024 configuration adds only 0.2–0.3 PPL above the FP16 baseline on all three models while compressing weights to 49–55% of the original size. Notably, Qwen3.5-9B-Base is especially resilient: even the aggressive 2-128 configuration maintains 7.65 PPL (vs. 6.98 FP16).

5.3.2 Comparison with Baselines. Table 2 presents a comprehensive comparison on Meta-Llama-3-8B, organized by model size.

¹<https://github.com/ist-daslab/gptq>

²<https://github.com/mit-han-lab/llm-awq>

³<https://github.com/mit-han-lab/smoothquant>

Table 2: Meta-Llama-3-8B: comparison of FASQ against quantization baselines, sorted by model size (% of FP16). FASQ requires no calibration data. Size% is measured from actual stored model weights. Best result per size region in bold. †Group size $g=128$.

Method	Calib Free?	#W	Size%	PPL↓	ARC-c	ARC-e	Hella	PIQA	Wino	Avg↑
FP16	–	16	100.0	6.14	50.3	80.1	60.2	79.5	73.7	68.8
<i>~49–57% size (FASQ near-lossless region)</i>										
SmoothQuant	✗	W8A8	56.6	6.3	49.0	79.6	60.0	79.4	73.2	68.2
SmoothQuant	✗	W6A6 [‡]	56.6	7.7	45.0	75.5	56.9	76.8	69.0	64.6
FASQ 2-1024	✓	5.0	49.0	6.3	49.7	79.0	59.9	78.9	73.3	68.2
<i>~35–42% size (FASQ vs INT4 region)</i>										
SmoothQuant	✗	W4A4	34.8	4.3E3	20.0	26.3	26.4	54.6	50.3	35.5
RTN [†]	✓	4	35.7	8.7	39.4	68.2	56.0	75.0	69.0	61.5
AWQ [†]	✗	4	35.7	6.6	48.5	79.3	59.1	78.6	73.1	67.7
GPTQ [†]	✗	4	35.7	6.5	47.7	78.8	59.0	78.4	72.6	67.3
QuIP	✗	4	34.8	6.5	47.4	78.2	58.6	78.2	73.2	67.1
FASQ 2-256	✓	4.0	37.0	6.7	48.0	79.5	58.5	79.4	73.4	67.8
FASQ 2-512	✓	4.5	41.9	6.4	50.0	78.5	59.5	78.7	73.4	68.0
<i>~29–33% size (FASQ vs INT3 region)</i>										
RTN [†]	✓	3	30.2	2.2E3	20.0	31.1	27.5	56.2	53.1	37.6
AWQ [†]	✗	3	30.2	8.2	43.2	74.0	55.1	77.7	72.1	64.4
GPTQ [†]	✗	3	30.2	8.2	37.7	70.5	54.3	74.9	71.1	61.7
QuIP	✗	3	29.4	7.5	41.0	72.9	55.4	76.8	72.5	63.7
FASQ 2-128	✓	3.5	33.2	7.4	46.3	77.1	56.4	78.2	72.2	66.0

✓ = calibration-free; ✗ = requires calibration data. [‡]W6A6 stored in INT8 containers; Size% reflects actual storage.

Table 3: FASQ compression and perplexity across model families. Size% = model size as percentage of FP16 baseline. PPL measured on WikiText-2 test set.

Config	Llama-3-8B		Qwen3-8B		Qwen3.5-9B	
	Size%	PPL↓	Size%	PPL↓	Size%	PPL↓
FP16	–	6.14	–	9.73	–	6.98
FASQ 2-1024	49.0%	6.34	50.5%	10.02	55.0%	7.06
FASQ 2-512	41.9%	6.48	43.4%	10.13	48.5%	7.13
FASQ 2-256	37.0%	6.81	38.6%	10.88	44.1%	7.29
FASQ 1-64	46.8%	6.88	48.1%	10.98	52.7%	7.31
FASQ 2-128	33.2%	7.57	34.8%	11.44	40.7%	7.65

Unlike baselines that are locked to discrete bit-widths (3/4-bit), FASQ covers a continuous range from 27% to 49% of FP16 size.

In the near-lossless region, SmoothQuant W8A8 (56.6% size, Avg 68.2) matches FASQ 2-1024 in quality, but FASQ achieves the same accuracy at 49% size, 8 percentage points smaller, and without calibration data. SmoothQuant W6A6, despite being stored in INT8 containers (also 56.6% actual storage), drops sharply to Avg 64.6. In the 4-bit region, FASQ 2-512 (41.9% size, Avg 68.0) and FASQ 2-256 (37.0% size, Avg 67.8) match GPTQ-4 g128 (35.7%, Avg 67.3) and QuIP-4 (34.8%, Avg 67.1), while SmoothQuant W4A4 collapses entirely (34.8%, Avg 35.5, PPL 4.3E3), demonstrating that

joint weight-activation quantization does not scale below 6-bit. This contrast highlights a fundamental advantage of FASQ’s product-quantization design: quality degrades gracefully across the entire compression range (68.2→68.0→67.8→66.0 from 49% to 33% size), whereas SmoothQuant has a single viable operating point (W8A8) and collapses below it (68.2→64.6→35.5). At 3-bit compression, FASQ 2-128 (33.2%, Avg 66.0) surpasses all 3-bit baselines including AWQ-3 g128 (30.2%, Avg 64.4) and QuIP-3 (29.4%, Avg 63.7). FASQ also uniquely extends below 3-bit: configuration 4-1024 reaches 31.1% size with Avg 66.4, a region no scalar baseline can access.

Critically, FASQ achieves all of these results *without any calibration data*, relying solely on k-means clustering of weight distributions, while every other baseline (GPTQ, AWQ, SmoothQuant, QuIP) requires a separate calibration pass on representative data. The entire FASQ quantization process (k-means over all layers) completes in approximately 10 minutes on a single GPU.

Table 4: Scalability of FASQ across LLaMA-2 model sizes.

Model	Config	Size%	PPL↓	Avg↑
7B	Baseline	–	5.47	64.1
	FASQ 1-64	41.2%	5.65	63.3
	FASQ 2-512	36.1%	5.55	63.8
	FASQ 4-1024	24.1%	6.04	61.5
13B	Baseline	–	4.88	66.5
	FASQ 1-64	40.0%	5.05	65.6
	FASQ 2-512	34.1%	4.94	66.3
	FASQ 4-1024	21.9%	5.36	65.0

5.3.3 Scalability. Table 4 demonstrates FASQ’s scalability from LLaMA-2 7B to 13B. Size% shrinks with model scale: the 4-1024 configuration reaches 24.1% at 7B and 21.9% at 13B, while PPL degradation remains modest (6.04 vs. 5.47 at 7B; 5.36 vs. 4.88 at 13B). This trend suggests that FASQ will be especially effective for larger models where the codebook overhead is further amortized.

5.4 End-to-End Inference Performance

Table 5 reports end-to-end latency on Meta-Llama-3-8B using real model inference on an RTX 3090. We compare FASQ against FP16 tensor-core inference and all baselines with their respective official inference kernels.

5.4.1 The Dequantization Overhead Problem. A key finding is that **weight-only quantization alone does not improve inference latency** compared to FP16 tensor-core execution. Naïve RTN quantization at 4-bit achieves only 10.4 tok/s decode, which is 4.2× slower than FP16 (43.9 tok/s), because the runtime must dequantize INT8 containers back to FP16 before calling cuBLAS, doubling the memory traffic and adding a full intermediate-materialization step. SmoothQuant W8A8 faces a similar bottleneck: despite using `torch._int_mm` for real INT8 GEMM on tensor cores, the per-token activation quantization and dequantization overhead limits decode to 16.4 tok/s (W6A6 is identical since it uses INT8 containers). Note that SmoothQuant targets a different tradeoff by quantizing both weights *and* activations; however, both W8A8 and W6A6 occupy 56.6% of FP16 in actual storage. At this cost, FASQ 2-1024 (49%, Avg 68.2) matches W8A8 quality in a smaller footprint, and far exceeds W6A6 (Avg 64.6). These results confirm that without specialized GPU kernel support, quantization can actually *hurt* latency.

5.4.2 Previous Work’s Fused Kernels. To overcome dequantization overhead, GPTQ and AWQ implement custom CUDA kernels that *fuse* weight unpacking with the matrix multiplication. AWQ’s W4A16 kernel [2] packs two 4-bit weights into one byte and fuses the unpack, dequantization, and FP16 GEMM into a single kernel launch, eliminating the intermediate FP16 weight materialization. GPTQ employs a similar fused-kernel strategy through optimized backends [1]. These fused kernels substantially improve over naïve dequantization: AWQ 4-bit achieves 28.1 tok/s decode (vs. RTN’s 10.4 tok/s) with 2.80× memory savings. However, even with kernel fusion, **no scalar quantization method matches FP16 decode**

speed (43.9 tok/s), because the dequantize-then-multiply paradigm inherently requires additional ALU operations per weight element.

5.4.3 FASQ Kernel Performance. In contrast, FASQ’s CUDA kernels (section 4) achieve FP16-parity decode speed while delivering substantial memory savings. At effective 4-bit precision ($SZ_{ss}=2$, $K_s=256$), FASQ achieves 45.2 tok/s decode, **surpassing FP16** (43.9 tok/s) while using **2.56× less memory** (5,975 MB vs. 15,317 MB). At effective 3-bit ($SZ_{ss}=2$, $K_s=128$), decode speed actually *exceeds* FP16 at 51.8 tok/s with 2.80× memory savings. This is possible because the GEMV kernel reads only the compact index table ($N_{ss} \times F_{out} = 8$ MB per layer at $SZ_{ss}=2$) rather than the full FP16 weight matrix (32 MB), achieving a 4× reduction in memory traffic that directly translates to proportional speedup in the memory-bandwidth-bound decode phase.

Compared to the best-performing baseline kernel, FASQ’s decode throughput is **1.6× faster** than AWQ 4-bit (45.2 vs. 28.1 tok/s), **2.2× faster** than GPTQ 4-bit (vs. 20.5 tok/s), **2.8× faster** than SmoothQuant W8A8 (vs. 16.4 tok/s), and **4.3× faster** than naïve RTN (vs. 10.4 tok/s). FASQ is the *only* compressed method that does not sacrifice decode speed for memory savings.

The prefill phase is slower than FP16 (935 ms vs. 41 ms at $K_s=256$) because the LUT-based GEMM cannot leverage tensor cores. However, in interactive serving the total latency is dominated by decode: at generation length 128, decode accounts for over 75% of end-to-end time, and this share grows with longer outputs. For deployments that prioritize time-to-first-token (TTFT), a hybrid dispatch that reconstructs FP16 weights for prefill via cuBLAS and switches to FASQ’s GEMV kernel for decode achieves both fast TTFT and compressed-model decode speed, at the cost of temporarily materializing the full weight matrix during prefill.

Table 5: End-to-end inference latency and memory on Meta-Llama-3-8B (RTX 3090, prompt/gen = 128 tokens).

Method	Mem (MB)	Prefill ms	tok/s	Decode ms/tok	tok/s	Mem Savings	Dec. Speedup
FP16 (Tensor Core)	15,317	40.8	3,137	22.8	43.9	1.00×	1.00×
SmoothQuant W8A8 [‡]	8,663	55.5	2,304	60.9	16.4	1.77×	0.37×
RTN (4-bit)	8,663	114.2	1,120	96.5	10.4	1.77×	0.24×
GPTQ (4-bit)	6,558	68.7	1,863	48.7	20.5	2.34×	0.47×
AWQ (4-bit)	5,463	75.1	1,705	35.6	28.1	2.80×	0.64×
RTN (3-bit)	8,671	118.2	1,083	96.9	10.3	1.77×	0.24×
GPTQ (3-bit)	5,808	94.0	1,362	75.9	13.2	2.64×	0.30×
AWQ (3-bit) [†]	5,463	75.1	1,705	35.6	28.1	2.80×	0.64×
<i>Eff. 4-bit ($SZ_{ss}=2$, $K_s=256$)</i>							
FASQ (reconstruct)	15,939	309.7	413	289.1	3.5	0.96×	0.08×
FASQ (Kernel)	5,975	934.9	137	22.1	45.2	2.56×	1.03×
<i>Eff. 3-bit ($SZ_{ss}=2$, $K_s=128$)</i>							
FASQ (reconstruct)	15,474	302.1	424	285.7	3.5	0.99×	0.08×
FASQ (Kernel)	5,482	761.9	168	19.3	51.8	2.80×	1.18×

[†]AWQ 3-bit reuses 4-bit containers; memory/latency identical to 4-bit. [‡]W6A6 uses INT8 containers; memory/latency identical to W8A8.

5.4.4 Structural Advantages. Beyond raw performance, FASQ offers two advantages that no scalar baseline provides. First, FASQ covers a continuous compression range from 27% to 49% of FP16

size by adjusting SZ_{ss} and K_s , all served by the *same* CUDA kernel, whereas scalar methods require a different kernel for each bit-width. Second, FASQ requires *zero calibration data*, eliminating distribution-mismatch risk and enabling instant quantization of any model, including proprietary ones where representative data is unavailable.

6 Conclusion

We presented FASQ, a calibration-free LLM compression framework based on product quantization. By tuning sub-vector size and codebook cardinality, FASQ spans 27–49% of FP16 model size with accuracy matching or exceeding GPTQ, AWQ, and SmoothQuant across Llama-3-8B, Qwen3-8B, and Qwen3.5-9B, all without calibration data. Our LUT-free GEMV kernel reduces memory traffic by 4× versus FP16, achieving 45.2 tok/s decode on an RTX 3090, surpassing FP16 (43.9 tok/s) at 2.56× less memory and outperforming every baseline kernel (1.6–4.3× faster). FASQ is the only compressed method that does not sacrifice decode speed for memory savings.

Limitations and future work. The prefill kernel remains slower than cuBLAS because LUT-based accumulation cannot leverage tensor cores. Two directions may close this gap: (1) a pipelined reconstruction kernel that rebuilds FP16 weight tiles in parallel with tensor-core GEMM, avoiding full materialization while exploiting hardware matrix units; and (2) Triton-based code generation with tiling strategies tailored to the PQ access pattern. On the compression side, per-layer parameter assignment and post-training codebook fine-tuning could further improve accuracy at aggressive compression rates.

References

- [1] Elias Frantar, Saleh Ashkboos, Torsten Hoefler, and Dan Alistarh. Gptq: Accurate post-training quantization for generative pre-trained transformers. *arXiv preprint arXiv:2210.17323*, 2022.
- [2] Ji Lin, Jiaming Tang, Haotian Tang, Shang Yang, Wei-Ming Chen, Wei-Chen Wang, Guangxuan Xiao, Xingyu Dang, Chuang Gan, and Song Han. Awq: Activation-aware weight quantization for llm compression and acceleration. In *MLSys*, 2024.
- [3] Guangxuan Xiao, Ji Lin, Mickael Seznec, Hao Wu, Julien Demouth, and Song Han. Smoothquant: Accurate and efficient post-training quantization for large language models. In *International Conference on Machine Learning*, pages 38087–38099. PMLR, 2023.
- [4] Yuxuan Wang, Ye Qiao, Sheldon Huang, and Hyoukjun Kwon. APEX-Q: Arbitrary-dimension product-EXTension quantization for accelerated LLM deployment. In *Proceedings of the AAAI Conference on Artificial Intelligence*, volume 40, page 41424, 2026.
- [5] Robert Gray. Vector quantization. *IEEE Assp Magazine*, 1(2):4–29, 1984.
- [6] Herve Jegou, Matthijs Douze, and Cordelia Schmid. Product quantization for nearest neighbor search. *IEEE transactions on pattern analysis and machine intelligence*, 33(1):117–128, 2010.
- [7] Davis Blalock and John Gutttag. Multiplying matrices without multiplying. In *International Conference on Machine Learning*, pages 992–1004. PMLR, 2021.
- [8] Jie Ran, Rui Lin, Jason Chun Lok Li, Jiajun Zhou, and Ngai Wong. Pecan: A product-quantized content addressable memory network. In *2023 Design, Automation & Test in Europe Conference & Exhibition (DATE)*, pages 1–6. IEEE, 2023.
- [9] Ting Chen, Lala Li, and Yizhou Sun. Differentiable product quantization for end-to-end embedding compression. In Hal Daumé III and Aarti Singh, editors, *Proceedings of the 37th International Conference on Machine Learning*, volume 119 of *Proceedings of Machine Learning Research*, pages 1617–1626. PMLR, 13–18 Jul 2020.
- [10] Xiaohu Tang, Yang Wang, Ting Cao, Li Lina Zhang, Qi Chen, Deng Cai, Yunxin Liu, and Mao Yang. Lut-nn: Empower efficient neural network inference with centroid learning and table lookup. In *Proceedings of the 29th Annual International Conference on Mobile Computing and Networking*, pages 1–15, 2023.
- [11] Ahmed Abouelhamayed, Angela Cui, Javier Fernandez-Marques, Nicholas Lane, and Mohamed Abdelfattah. Pqa: Exploring the potential of product quantization in dnn hardware acceleration. *ACM Transactions on Reconfigurable Technology and Systems*, 18(1):1–29, 2024.
- [12] Guoyu Li, Shengyu Ye, Chunyun Chen, Yang Wang, Fan Yang, Ting Cao, Cheng Liu, Mohamed M Sabry Aly, and Mao Yang. Lut-dla: Lookup table as efficient extreme low-bit deep learning accelerator. In *2025 IEEE International Symposium on High Performance Computer Architecture (HPCA)*, pages 671–684. IEEE, 2025.
- [13] Ye Qiao, Zhiheng Chen, Yifan Zhang, Yian Wang, and Sitao Huang. Tellme: An efficient end-to-end ternary llm prefill and decode accelerator with table-lookup matmul on edge fpgas. In *Proceedings of the 2026 ACM/SIGDA International Symposium on Field Programmable Gate Arrays*, pages 247–257, 2026.
- [14] Yufei Zhang, Zheyu Chen, Ye Qiao, and Sheldon Huang. PD-Swap: Prefill-decode logic swapping for end-to-end LLM inference on edge FPGAs via dynamic partial reconfiguration. *arXiv preprint arXiv:2512.11550*, 2025.
- [15] Ye Qiao, Zhiheng Chen, Yian Wang, Yifan Zhang, Yunzhe Deng, and Sitao Huang. Cobra: Algorithm-architecture co-optimized binary transformer accelerator for edge inference. In *2025 IEEE/ACM International Conference On Computer Aided Design (ICCAD)*, pages 1–8. IEEE, 2025.
- [16] Ye Qiao, Haocheng Xu, Yifan Zhang, and Sitao Huang. Micronas: Zero-shot neural architecture search for mcus. In *2024 Design, Automation & Test in Europe Conference & Exhibition (DATE)*, pages 1–2. IEEE, 2024.
- [17] Ye Qiao, Hongwei Xu, Yufei Zhang, and Sheldon Huang. MONAS: Efficient zero-shot neural architecture search for MCUs. In *International Joint Conference on Neural Networks (IJCNN)*, pages 1–8, 2025.
- [18] Ye Qiao, Jingyi Li, Hongwei Xu, and Sheldon Huang. TG-NAS: Generalizable zero-cost proxies with operator description embedding and graph learning for efficient neural architecture search. *arXiv preprint arXiv:2404.00271*, 2024.
- [19] Ye Qiao, Ao Ding, and Nader Bagherzadeh. BNN an ideal architecture for acceleration with resistive in memory computation. *IEEE Transactions on Emerging Topics in Computing*, 11(2):281–291, 2023.
- [20] Hongwei Xu, Fatemeh Tahmasebi, Ye Qiao, Haoyu Tian, Hyoukjun Kwon, and Sheldon Huang. Optimized spatial architecture mapping flow for transformer accelerators. *arXiv preprint arXiv:2410.07407*, 2024.
- [21] Ye Qiao and Sheldon Huang. Q-ROAR: Outlier-aware rescaling for RoPE position interpolation in quantized long-context LLMs. In *Proceedings of the AAAI Conference on Artificial Intelligence*, volume 40, page 41359, 2026.
- [22] Ye Qiao, Hongwei Xu, Xing Zhang, and Sheldon Huang. Rethinking RoPE scaling in quantized LLM: Theory, outlier, and channel-band analysis with weight rescaling. *arXiv preprint arXiv:2510.00028*, 2025.
- [23] Jerry Chee, Yaohui Cai, Volodymyr Kuleshov, and Christopher De Sa. Quip: 2-bit quantization of large language models with guarantees. In *Advances in Neural Information Processing Systems*, volume 36, 2023.
- [24] Aaron Grattafiori, Abhimanyu Dubey, Abhinav Jauhri, Abhinav Pandey, Abhishek Kadian, Ahmad Al-Dahle, Aieleen Letman, Akhil Mathur, Alan Schelten, Amy Yang, et al. The llama 3 herd of models. *arXiv preprint arXiv:2407.21783*, 2024.
- [25] Qwen Team. Qwen3, April 2025.
- [26] Hugo Touvron, Louis Martin, Kevin Stone, Peter Albert, Amjad Almahairi, Yasmine Babaei, Nikolay Bashlykov, Soumya Batra, Prajjwal Bhargava, Shrusti Bhosale, et al. Llama 2: Open foundation and fine-tuned chat models. *arXiv preprint arXiv:2307.09288*, 2023.
- [27] Stephen Merity, Caiming Xiong, James Bradbury, and Richard Socher. Pointer sentinel mixture models. *arXiv preprint arXiv:1609.07843*, 2016.
- [28] Peter Clark, Isaac Cowhey, Oren Etzioni, Tushar Khot, Ashish Sabharwal, Carissa Schoenick, and Oyvind Tafjord. Think you have solved question answering? try arc, the ai2 reasoning challenge. *arXiv preprint arXiv:1803.05457*, 2018.
- [29] Rowan Zellers, Ari Holtzman, Yonatan Bisk, Ali Farhadi, and Yejin Choi. Hellaswag: Can a machine really finish your sentence? *arXiv preprint arXiv:1905.07830*, 2019.
- [30] Yonatan Bisk, Rowan Zellers, Jianfeng Gao, Yejin Choi, et al. Piqa: Reasoning about physical commonsense in natural language. In *Proceedings of the AAAI conference on artificial intelligence*, volume 34, pages 7432–7439, 2020.
- [31] Keisuke Sakaguchi, Ronan Le Bras, Chandra Bhagavatula, and Yejin Choi. Winogrande: An adversarial winograd schema challenge at scale. *Communications of the ACM*, 64(9):99–106, 2021.
- [32] Leo Gao, Jonathan Tow, Baber Abbasi, Stella Biderman, Sid Black, Anthony DiPofi, Charles Foster, Laurence Golding, Jeffrey Hsu, Alain Le Noac’h, Haonan Li, Kyle McDonell, Niklas Muennighoff, Chris Ociepa, Jason Phang, Laria Reynolds, Hailey Schoelkopf, Aviya Skowron, Lintang Sutawika, Eric Tang, Anish Thite, Ben Wang, Kevin Wang, and Andy Zou. The language model evaluation harness, 07 2024.